Journal of Structural Biology 177 (2012) 233–238

Contents lists available at SciVerse ScienceDirect

Journal of Structural Biology

journal homepage: www.elsevier.com/locate/yjsbi

X-ray mosaic nanotomography of large microorganisms

R. Mokso [a,*], L. Quaroni [a], F. Marone [a], S. Irvine [a,b], J. Vila-Comamala [c], A. Blanke [d], M. Stampanoni [a,e]

[a] Swiss Light Source, Paul Scherrer Institut, 5232 Villigen, Switzerland
[b] School of Biology and Medicine, University of Lausanne, Switzerland
[c] Laboratory for Micro- and Nanotechnology, Paul Scherrer Institut, 5232 Villigen, Switzerland
[d] Zoologisches Forschungsmuseum Alexander Koenig, Adenauerallee 160, 53113 Bonn, Germany
[e] Institute for Biomedical Engineering, University of Zürich and ETH Zürich, 8092 Zürich, Switzerland

ARTICLE INFO

Article history:
Available online 29 December 2011

Keywords:
X-ray microscopy
Bacteria
Synchrotron
Tomography
Phase-contrast

ABSTRACT

Full-field X-ray microscopy is a valuable tool for 3D observation of biological systems. In the soft X-ray domain organelles can be visualized in individual cells while hard X-ray microscopes excel in imaging of larger complex biological tissue. The field of view of these instruments is typically 10^3 times the spatial resolution. We exploit the assets of the hard X-ray sub-micrometer imaging and extend the standard approach by widening the effective field of view to match the size of the sample. We show that global tomography of biological systems exceeding several times the field of view is feasible also at the nanoscale with moderate radiation dose. We address the performance issues and limitations of the TOMCAT full-field microscope and more generally for Zernike phase contrast imaging. Two biologically relevant systems were investigated. The first being the largest known bacteria (*Thiomargarita namibiensis*), the second is a small myriapod species (*Pauropoda* sp.). Both examples illustrate the capacity of the unique, structured condenser based broad-band full-field microscope to access the 3D structural details of biological systems at the nanoscale while avoiding complicated sample preparation, or even keeping the sample environment close to the natural state.

1. Introduction

The penetrating power of X-rays coupled to the high photon flux of 3rd generation synchrotron sources makes X-ray tomography outperform other imaging techniques in particular when large, opaque samples need to be investigated with high spatial and temporal resolution. Standard synchrotron-based-microtomography, reaching about 1 μm spatial resolution (Stampanoni et al., 2010), does not allow the imaging of samples down to the cellular level in sufficient detail. There is a general need to overcome this limitation and to further develop imaging techniques reaching sub-micrometer spatial resolution. The performance of full-field X-ray microscopy instruments relies on the fabrication of X-ray optical components, like Fresnel zone plates (FZP) used as beam shapers, condensers or magnifying lens, similar to visible light microscopes. The main difference is that for a FZP-based X-ray microscope, the spatial resolution is mainly affected by the size of the outermost zone of the lens rather than by the diffraction constraints. The fabrication of X-ray lenses is technologically challenging especially for hard (>10 keV) X-rays. This explains the apparently paradox situation of state-of-the-art X-ray microscopes, where the best achieved spatial resolution is inversely proportional to the X-ray wavelength at which the full-field microscope operates. Soft X-ray full-field microscopes look back to a longer history and can currently achieve a spatial resolution of about 20 nm routinely (Parkinson et al., 2008). They are typically designed to work in the water window (283–530 eV) and the contrast is based on absorption using the significant difference in photoelectric cross-section between carbonized structure and the aqueous medium. The small penetration depth – typically less than 15 μm for biological soft tissue – is sufficient to study single cells. On the other hand, hard X-ray microscopes with efficient tomographic capabilities usually operate in projection mode (Mokso et al., 2007) or full-field mode (Andrews et al., 2010; Neuhausler et al., 2003) and typically in the range of 6–20 keV with a penetration depth of up to several millimeters, granting therefore insight into larger samples made of materials with higher atomic numbers. In projection mode at 17–29 keV, with inherent propagation-based phase contrast, a spatial resolution of 180 nm in 3D has been reported in Requena et al. (2009). In full-field mode and Zernike phase contrast a spatial resolution of 30 nm was demonstrated for the 2D case in Chen et al. (2011) and beyond 200 nm for 3D in Stampanoni et al. (2010) and Takeuchi et al. (2011). As

* Corresponding author. Address: WBBA/214, Paul Scherrer Institut, 5232 Villigen, Switzerland.
E-mail address: rajmund.mokso@psi.ch (R. Mokso).
URL: http://psi.ch (R. Mokso).

1047-8477/$ - see front matter © 2012 Elsevier Inc. All rights reserved.
doi:10.1016/j.jsb.2011.12.014

a consequence and differently from soft X-ray microscopes these instruments are well suited for both biological and material science applications. A more detailed review on X-ray microcopy can be found in Sakdinawat and Attwood (2010). Here, we highlight two biological applications of a full-field hard X-ray Zernike phase contrast microscope based on a structured condenser and its corresponding, custom-designed X-ray phase shifting optical component. We fully exploit the large penetration length and depth of focus as well as the short exposure times to perform full-field 3D nanoimaging of large biological objects that we will refer to as "mosaic tomography".

2. Instrumentation and methods

The TOMCAT beamline of the Swiss Light Source (Stampanoni et al., 2010) operates a full-field microscope with moderately monochromatic X-ray beam from a double crystal multilayer monochromator ($\Delta\lambda/\lambda = 10^{-2}$). The advantage of this unusual choice for the energy bandwidth is the high photon flux from the multilayer ensuring short exposure times and therefore fast data collection. The benefit is evident, in particular for tomographic acquisitions, where a large number of angular projections is required and therefore shorter exposure times results in relaxed requirements on the instrumentation's long term stability. Fast data acquisition is a particularly important prerequisite for realizing full-field raster scanning in order to extend the effective field of view of the microscope. This can be done in either 2D (Andrews et al., 2008) or, as introduced in this work, in 3D (mosaic tomography).

2.1. The optical layout

The TOMCAT full-field microscope is operated optimally between 8 and 12 keV, since for this energy range the efficiency of each diffractive optical element lies between 6% and 9% while it significantly decreases at higher energies. For this work in particular, we adjusted the X-ray energy to 10 keV. As described in detail in Stampanoni et al. (2010) and schematically shown in Fig. 1, the beam condenser installed 20 m downstream from the source (13 m from the Ru/C multilayer monochromator) collects 1×1 mm^2 of the X-ray beam and creates a sample illumination of 0.05×0.05 mm^2 at a distance of $f_{condenser}$ = 760 mm further downstream. The unconventional design by Jefimovs et al. (2008) of this structured condenser results in a square top-flat illumination spot instead of the most common circular one with an Airy disk profile. We use a condenser with an outermost zone width of 70 nm. Gold structures of 900 nm in height have been fabricated by electroplating into a polyimide mould. The resulting aspect-ratio of 13 ensures about 8% diffraction effciency. To obtain a homogeneous, top-flat illumination with this structured condenser (Fig. 1b), the transverse coherence length of the incoming X-rays should be smaller than the size of one single element within the condenser lens. In our case, one structural element is 50×50 μm^2 in size and therefore, at 20 m from the superbend source, the above mentioned condition is satisfied along both the vertical and horizontal direction. For broad bandwidth illumination, the depth of focus of the condenser is several hundreds of micrometers long. This can be verified experimentally (Fig. 2) by recording a through-focus series around the condenser focal plane. As a consequence, large samples are illuminated uniformly not only along the lateral but even along the direction of the optical axis. To produce a magnified image of the sample ($d_{detector}$ = 9.95 m downstream of the lens), an objective zone plate is inserted 56.8 mm downstream the sample. We use a Fresnel zone plate with 70 nm outermost zone width and 900 nm high gold structures, this time lithographically prepared on a thin SiN membrane. With a

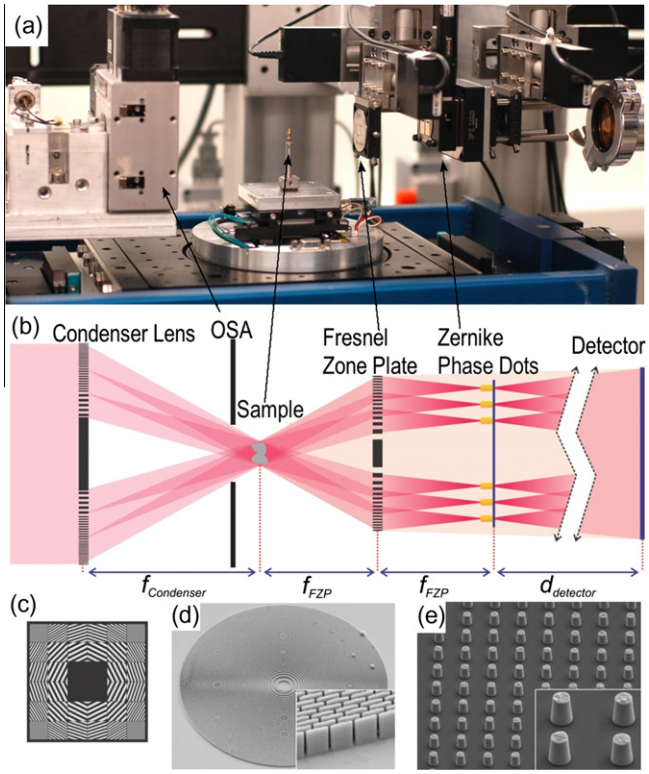

Fig.1. The TOMCAT nanoscope (a) with the schematic drawing of the layout (b) and the structured condenser (c). SEM images of the objective Fresnel zone plate and (d) and the phase dots (pillars) (e)

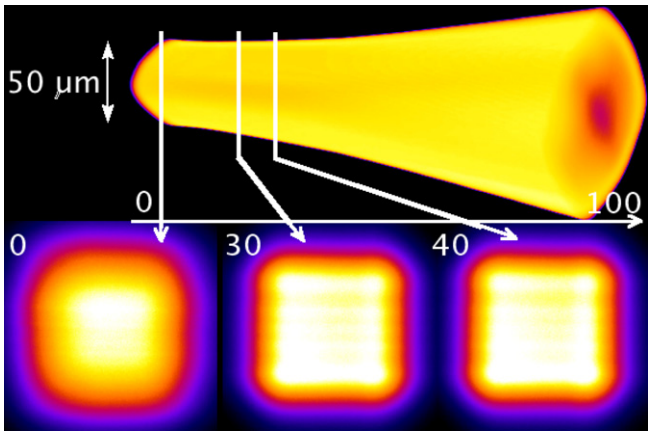

Fig.2. The illumination cone near the focal plane of the condenser acquired using a high resolution X-ray detector over 100 mm in beam direction with a step size of 1 mm. The three transversal beam profiles in the lower part of the Figure are shown for the positions 0, 30 and 40 mm.

diameter of 100 μm the focal distance at 10 keV is f_{FZP} = 56.4 mm. The numerical aperture is matched to that of the condenser ensuring therefore best performance (Goodman, 1988). A 14-bit dynamic range and high sensitivity Photonics Science VHR water cooled CCD detector is coupled via a fiber optics taper (with 3-fold magnification) to the scintillator screen (GdOS:Tb). The geometrical pixel size at the scintillator plane is 4 μm. Accounting for the magnification of the X-ray microscope of M = 175, the pixel size of the full-field X-ray microscope is 23 nm. In this configuration the (absorption) contrast in the images arises through the variation of the photoelectric cross section of the elements composing the sample. However,

the majority of small samples investigated at submicrometer resolution exhibit naturally very little attenuation contrast at 10 keV due to their small size. Especially for biological samples, an alternative, more sensitive, approach is desired. Zernike phase contrast (ZPC) (Zernike, 1934) offers improved sensitivity. We generate ZPC by inserting an array of phase shifting gold pillars in the back-focal plane of the Fresnel zone plate. These are lithographically fabricated on a thin SiN membrane and consist of 25×25 pillars spaced by 3.56 μm. Their diameter is 0.9 μm and their height 3 μm. This specific array scheme is required to match the shape of the condenser's illumination in the Fourier space, where each of its individual structural element corresponds to a light spot. In the following, we will refer to this optical element as Zernike phase dots as introduced in Stampanoni et al. (2010).

2.2. Formation and interpretation of Zernike phase contrast images

Zernike phase contrast is an interferometric technique where the reference and object wave are spatially not separated and belongs therefore to the common-path interferometric methods. The reference wave is the part of the beam which is not affected by the sample: it constitutes the transmitted, undiffracted part of the beam. There are three distinct arrangements which give rise to ZPC-type interference. The first – most commonly used – is by retardation of the reference wave (*positive* ZPC), the second is by retardation of the diffracted part of the beam (*negative* ZPC) and the last option is by attenuating the reference wave. In Stampanoni et al. (2010) we showed the performance of a full-field microscope operated in negative ZPC mode while in the current study we present a combination of the first and third option to produce positive ZPC images enhanced by reference beam attenuation. The positive ZPC image is produced with a $\pi/2$ phase shift combined with the attenuation of the reference wave via the Zernike phase dots and – at the same time – by letting the beam diffracted by the sample travel unchanged and in turn create interference with the delayed diffracted branch. Different phase shifting dots (e.g. $\pi/4$ or $3\pi/4$) can also be used to manipulate the image contrast. In this paper, for the sake of simpler interpretation of the intensity values, we use the $\pi/2$ phase shift. If we write the complex object function as $T(x,y) = A \cdot exp(i\phi)$ and suppose a pure phase object satisfying the weak phase approximation (sometimes referred to as small-scale phase approximation) then the complex object function can be approximated by the Taylor expansion to the first order as $T(x,y) = 1 + i\phi$. The intensity in the images may then be linearly mapped to the actual phase of the object. In the case of a $\pi/2$ phase dots it becomes $I = i + 2\phi$.

2.3. Sample requirements

When using 10 keV X-rays the penetration depth in biological tissue is as great as several millimeters. Furthermore, because the depth of focus for the X-ray lenses is several hundred micrometers too, an X-ray projection image (2D) of large (several hundred micrometers) samples can therefore be acquired and interpreted. In standard X-ray Zernike Phase Contrast microscopy meaningful 3D images are obtained, if the samples lateral dimensions are restricted to approximately the field of view of the microscope, in our case 40 μm. As discussed above, the image contrast generated by a Zernike type microscope can – under the condition of weakly absorbing objects – be linearly related to the phase shifting properties of the sample. Practically, this condition means that the sample must produce a phase shift smaller than $\pi/3$ (Goodman, 1988) for the first order Taylor expansion to be valid. If such requirements are not met and the object is violating the first-order Taylor approximation, then it is no longer straightforward to extract quantitative information from ZPC images either in 2D or in 3D. The possibility to use a Taylor expansion to higher orders was theoretically investigated by Teschke and Sinzinger (2009). An alternative method based on Fourier decomposition was attempted by Glückstad and Palima (2009). It is mainly in visible light microscopy where efforts are put into the quantitative interpretation of ZPC images of strong phase objects while for ZPC with X-rays the imaging of strong phase objects remains in many studies rather qualitative than quantitative.

2.4. Data processing

The raw tomographic projections are corrected for the background and detector dark current using the usual expression (*Image-dark*)/(*background-dark*). Other than this the projections do not undergo further processing prior to the tomographic reconstruction. In the case of the mosaic tomography the projections corresponding to a given angular position are stitched to form a single projection image. The stability of the microscope and the precision of the sample stages allow one to feed the angular projections directly into the standard tomographic reconstruction algorithms. The Fourier based tomographic reconstruction routine (Marone et al., 2008) used for parallel beam tomography at the TOMCAT beamline was applied to all data. The resulting volumes capture the spatial distribution of structures based on their phase retardation action on the probing X-rays. The images shown in the figures are raw data without further manipulation.

2.5. Radiation dose

One important issue to address in X-ray microscopy is the deposited dose and its effects on the samples. It has been established that the deposited dose is a function of the desired spatial resolution (Howells et al., 2009). Particularly for biological samples, images are strongly affected by radiation issues and are mainly showing the damaged tissue rather than its natural state. Specifically for our experiment at 10 keV, the photon flux incident on the condenser is approximately 10^{11} photons/s/mm^2. Accounting for the efficiency and focal spot size of the condenser as well as the 0.6×0.6 mm^2 beam blocker, the total photon flux within the illumination plane reaches 10^{12} photons/s. Because only about 8% of these photons at 0.12 nm wavelength are absorbed in the bacteria, the deposited dose rate – calculated according to the simplified model reported by Howells et al. (2009) – is below 1 Gy/s. According to the empirical formula $D_{mt}[\text{Gray}] = 10^8 \cdot res[\text{nm}]$ (Howells et al., 2009), where *res* is the spatial resolution, the maximum tolerable dose for a spatial resolution of 100 nm is $D_{\text{mt}} = 10^{10}$ Gray. To verify the non-destructive features of our hard X-ray 3D microcopy technique, we captured an image of the sample (*T. namibiensis* as discussed in Section 3.1) before and after the tomographic acquisition and compared them in order to investigate eventual damage in the structure. Taking into account the total exposure time during the tomographic acquisition as described below the calculated dose deposited into the bacteria is less than 70 Grays, i.e. well below the tolerable radiation.

3. Results

In this work, we focus on two examples of large (several hundreds of micrometers) biological specimens to demonstrate the unique capabilities of mosaic, hard X-ray full-field microscopy in Zernike phase contrast mode. The first example is a bacterium (*T. namibiensis*), the second is a myriapod insect (*Paurupoda* sp.). The experiments were performed with a pixel size of 46 nm. For this configuration the 3D spatial resolution previously evaluated in Stampanoni et al. (2010) is 144 nm. In each of the two

applications the spatial resolution was addressed separately in a similar way.

3.1. T. namibiensis bacteria

Thiomargarita bacteria are the largest known bacteria, with individual cells typically 100–300 μm in diameter, but reaching a size of up to 700 μm Schulz et al., 1999; Schulz and Schulz, 2005. The cells are often gathered to form chains that are visible to the naked eye. Thiomargarita are lithotrophic organisms living in oceanic sediments, where they survive by oxidizing hydrogen sulfide using nitrate stored in a large vacuole. The cell structure is dominated by the vacuole, with the cytoplasm limited to a thin (about 2 μm) surrounding layer. Strings of bacterial cells are further enveloped by a gelatinous sheath. The sheath is believed to protect the cell from mechanical damage arising from contact with sediment particles. As part of their metabolism, the bacteria accumulate inclusions of elemental sulfur, polyphosphate and polyglucose, ranging in size from 1 to 10 μm, distributed over a roughly spherical surface at the periphery of the cell. We observed that the larger inclusions are spherical and their size distribution in the studied bacteria was very monodisperse with a diameter of 4 μm. The absorption of such particles, presumably sulfur according to their size, at 10 keV is only about 4%. They shift the phase by $\pi/4$ at most (when X-rays travel through their center) satisfying locally the condition for quantitative ZPC imaging at 10 keV, yet their transmission for soft X-rays (water window) would still be less than 1% making their observation with a soft X-ray microscope practically impossible.

The bacteria are not mobile, so no mobility preventing substances such as gels or fixatives had to be used. The sample preparation consists therefore only of inserting the bacteria into a capillary of 300 μm in diameter, containing seawater and marine sediment, and placing the capillary onto the sample stage. Nonetheless some sporadic movements of the cell have been occasionally observed, probably due to convection processes within the medium in the capillary.

Fig. 3a depicts a 2D mosaic image resulting from raster scanning the sample in full-field microscopy mode. A total of $9 \times 20 = 180$ radiographic images were collected covering the whole area of the sample with a lateral extension of approximately 200 μm. The exposure time for each radiographic projection was 1.4 s (for 2× binning and a pixel size of 46 μm). This procedure can be applied at any selected angular positions (Fig. 3b is rotated 45° around the tomographic rotation axis as compared to Fig. 3a). For the demonstration of the proposed low dose mosaic tomography mode we selected a horizontal 'stripe' of 1×6 fields of view Fig. 3c to form a single, stitched projection for 73 angular positions, i.e. one stripe every 180/72°. Finally, we combined the raster scanning of 1×6 FOV with the rotation of the bacteria around the vertical tomographic axis. This results in a set of 73 radiographic projections each of 700×4200 pixels corresponding to the physical dimensions of 35×210 μm for the final FOV. The total exposure time during which the bacteria was irradiated was 12 min for the whole tomographic set, not including overheads introduced by the movement of the linear stages and the readout time for the CCD.

Applying the standard reconstruction routine (Marone et al., 2008) we obtain a tomogram of the entire horizontal size of the bacteria. In this particular application we chose to minimize the deposited radiation dose on the bacteria and compromise the true 3D spatial resolution as it is affected by the angular undersampling (small amount of tomographic projections). The power spectrum method applied on the whole reconstructed 3D volume gives a spatial resolution of 150 and 210 nm in the directions parallel and perpendicular to the tomographic rotation axis, respectively. The image (Fig. 3b) shows in detail the distribution of inclusions at the periphery of the cell. This is the first time that the accurate mapping of the inclusions of Thiomargarita in 3D has been reported. Previous measurements used confocal fluorescence microscopy to visualize the distribution of the cytoplasm. TEM experiments also provided high resolution images of the cytoplasm (Schulz, 2006), but at the expense of dissolving sulfur grains during the fixation process. Rotation of the image clearly shows the distribution of the inclusions along a spherical surface, which cannot be appreciated from a single 2D projection. Spherical inclusions larger than 3 microns in size are expected to be mostly elemental sulfur. Smaller irregular inclusions could be either polyphosphates or polyglucose deposits.

The inorganic components of the sheath are also imaged with high contrast and high resolution. Several diatom and foraminifera

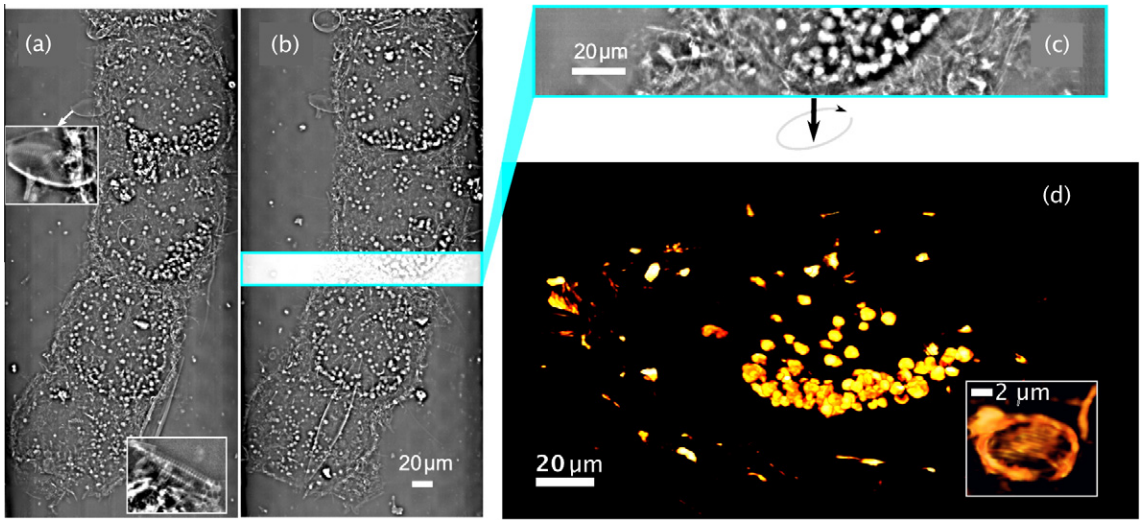

Fig.3. Mosaic tomographic nanoimaging of the Thiomargarita namibiensis bacteria. In (a) and (b) are depicted the 2D mosaic images, at 0° and 45°, respectively, consisting of 9×20 radiographic images obtained through raster scanning the sample in full-field microscopy mode. In (c), we show an example of the row of 1×6 images used for the tomography. By combining 73 angular positions, the result is a 3D reconstruction with rendering shown in (d). Amongst other information, we are able to see for the first time an accurate distribution in 3D of the inclusions at the periphery of the cell. The insets in (a) represent zoomed-in projection images of diatoms attached to the surface of the bacteria. The inset in (d) highlights a 3D rendering of a diatom zoomed in at the tomographic reconstruction to appreciate its fine structure.

skeletons attached to the gelatinous sheath have been easily identified. For some of them, fine structural patterns of the skeleton could be appreciated with submicron resolution as highlighted in the insets of Fig. 3a and d. In addition to these well identified structures, numerous small structures are seen embedded in the sheath, probably representing fragments of shells.

We also investigated the radiation damage and, as all images before and after the scanning procedure were identical, we therefore conclude that no obvious radiation induced damage was observed on the bacteria.

3.2. Micro-arthropods (Pauropoda sp.)

The aim of our second example is the visualization of internal structures in micro-arthropods. Nanotomography can be particularly useful for imaging muscles and cuticular structures in these animals. It delivers fast, consistent results with good resolution allowing for structure comparison between many taxa in a reasonable timeframe. In particular, this feature was used here to study soil dwelling micro-arthropods. The single species shown in the present work forms a part of a bigger framework aiming at a detailed comparison of the leg and trunk musculature of all major myriapod taxa. Leg and trunk musculature has proven useful to infer phylogenies of other Arthropoda (Bäcker et al., 2008). Myriapoda (centipedes) are a subphylum of the megadiverse arthropods (a phylum containing also insects, arachnids and crustaceans, approximately 1.2 million of described species). Despite numerous molecular research activities (Gai et al., 2006; Regier et al., 2005; SPS Name, SPS Year) the phylogeny of Arthropoda, in particular the location of myriapods is still heavily disputed. Myriapods are composed of four main taxa (Chilopoda, Diplopoda, Pauropoda and Symphyla) whose intrarelationships are also not clear. This situation requires a broad taxon sampling, so that character polarisation can be developed robustly.

As an example, we present here *Pauropus* sp. (Pauropoda), a particular small taxon of Myriapoda (approximately 0.5×1 mm body size). The legs of these species are extremely small (ca. 0.2×0.1 mm). Prior to scanning, samples were dried at the critical point (CPD) (Model E4850, BioRad) and mounted on dedicated specimen holders. Similarly to the previous example, we raster scanned and stitched the images of the whole insect to identify the regions of interest for the individual nanotomographic acquisitions (Fig. 4a). The scale bar of 40 μm is chosen to highlight the standard field of view of the instrument. When the regions of interest were identified, a tomographic set of the femur articulation was acquired. Differently from the previous example, the scanning procedure here was the standard one consisting of 460 projections (without raster scanning). The tomographic reconstruction was performed using the standard algorithm for parallel beam. Subsequent segmentation and rendering was accomplished with GPL license packages Reconstruct (Fiala, 2005) and Blender (blender.org). The 3D spatial resolution evaluated on tomographic slices of various orientation using the power spectrum analysis corresponds to 140 nm similarly to the previously published results Stampanoni et al., 2010. The high 3D spatial resolution allows one to observe fine structural details as demonstrated in Fig. 4e.

The 3D reconstructions clearly show the cuticle and musculature at the femur-postfemur articulation (Fig. 4b-e) as well as connective tissue and membranes. The last accounts of these body parts date back several decades (Tiegs, 1947). From the rendering on Fig. 4b–d and the movie in the Supplementary material it becomes obvious that the muscle equipment differs from the literature record. The tarsal flexor (tfl) originates clearly not in the femur. The post-femur flexor (pffl, "fl.tb") in Tiegs (1947) is composed of two muscle bundles instead of three (Tiegs, 1947). This gives important information about the development of character matrices which can be subsequently used for phylogenetic analysis. Moreover, it became apparent that the large bristle at the dorsal side of the femur is connected to the large tarsal flexor (Fig. 4d); tfl) by connective tissue. The structural linkage may be of importance for rapid motions of the leg, not controlled by the nervous system, but by indirect stimuli. If the bristle is deflected by an

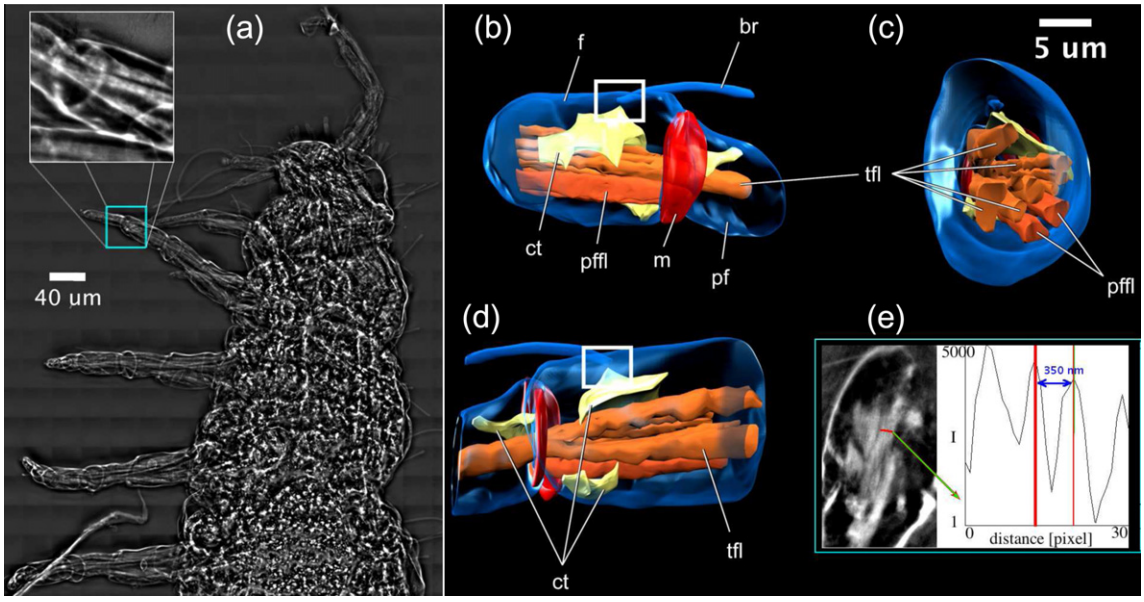

Fig.4. Stitched 2D image of the *Pauropus* sp. (Myriapoda) showing the habitus of the animal. The inset in (a) represents a projection image of the selected region of interest for the tomographic acquisition. On the right the volume rendering of the tomographic reconstruction of the femur-postfemur articulation with detailed labeling of the different muscle groups are shown. The colormap highlights the cuticle (blue, partly transparent), muscles (orange), connective tissue (yellow), and membranes (red). The three dimensional reconstruction is visualised by the anterior view (b), mesolateral view (c) and posteroir view (d). White square highlights the connection between bristle and connective tissue. Further explanations see text. Abbreviations: br, bristle; ct, connective tissue; f, femur; m, membrane; pf, post-femur; pffl, post-femur flexor; tfl, tarsal flexor. In (e) the spatial resolution and tissue contrast is demonstrated. The line profile (on the right) along a 2 μm long line (in red) on a tomographic slice (on the left) highlights the resolved fine structure of the connective tissue. The *Y*-axis represents the normalized gray value in the reconstructed 16 bit tomographic slice.

obstacle in the way of this leg part, the deflection is transferred via the connective tissue to the tarsal flexor. This induces a contraction of this muscle so that the tarsus is flexed rapidly to react to objects which are in the way of the leg. Such indirectly controlled movements are frequently reported for arthropods, but are not known for Pauropoda, yet (Koditschek et al., 2004). It remains to be tested by further studies which precise impact this morphological linkage, identified here for the first time, has for the functional biology of pauropod legs.

4. Conclusions

In this paper, we discuss the performance and limitations of the hard X-ray full-field microscope in Zernike phase contrast mode. With two biologically relevant examples we show how large samples can be characterized in 3D at the nanoscale.This type of sample has so far been visualized with mostly surface sensitive methods in 2D (visible light microscopy, SEM) or with limited spatial resolution in 3D (parallel beam X-ray imaging). For both cases the fast mosaic radiographic imaging is first used to identify the regions of interest. This is followed either by standard nanoscale tomography or (as introduced in this paper) by mosaic tomography to access the spatial distribution of relevant features in 3D within the selected region of interest. With the study of *T. namibiensis* we demonstrated the capability to perform 3D nanoscale imaging with an extended field of view up to the lateral dimension of the sample rather than performing local tomography. The Thiomargarita bacteria was scanned in an environment of seawater with sediments, i.e. very close to its natural condition. This fact can be of utmost importance for many biological studies where complicated sample preparation can impair the purpose of the study, since biological systems do often change their structure/functionality when extracted from their natural environment. Hard X-rays are a highly efficient probe for sub-micrometric 3D imaging of relatively large biological samples and in particular when anorganic compounds are part of the inner structure. It must be pointed out that today there is no alternative technique to hard X-ray microscopy to extract the 3D structural details at the nanoscale for these two kinds of applications.

5. Outlook

In our setup it is straightforward to switch between positive and negative ZPC simply by substituting the phase pillars by phase 'holes'. As shown in this and in an earlier work (Stampanoni et al., 2010) both configurations give similar image quality. Therefore the linear combination of a doublet of positive and negative ZPC images could further enhance the image contrast if desired. For the low dose mosaic tomography, iterative tomographic reconstruction methods may bring improvement in image quality.

Acknowledgments

We greatly acknowledge G. Mikuljan of the SLS- TOMCAT beamline staff for his fundamental support in setting up the experiment. This study was supported by Centre d'Imagerie BioMedicale (CIBM) of the UNIL, UNIGE, HUG, CHUV, EPFL and the Leenaards and Jeantet Foundations.

Appendix A. Supplementary data

Supplementary data associated with this article can be found, in the online version, at doi:10.1016/j.jsb.2011.12.014.

References

Andrews, J.C., Almeida, E., van der Meulen, M.C., Alwood, J.S., et al., 2010. Nanoscale X-ray microscopic imaging of mammalian mineralized tissue. Microscopy and Microanalysis 16, 327–336.
Andrews, J.C., Brennan, S., Patty, C., Luening, K., Pianetta, P., et al., 2008. A high resolution, hard X-ray bio-imaging facility at ssrl. Synchrotron Radiation News 21, 17–26.
Bäcker, H., Fanenbruck, M., Wägele, J.W., 2008. A forgotten homology supporting the monophyly of Tracheata: the subcoxa of insects and myriapods re-visited. Zoologischer Anzeiger – A Journal of Comparative Zoology 247, 185–207.
Chen, Y.T., Chen, T.Y., Yi, J., Chu, Y.S., Lee, W.K., et al., 2011. Hard X-ray zernike microscopy reaches 30 nm resolution. Optics Letters 36, 1269.
Fiala, J.C., 2005. Reconstruct: a free editor for serial section microscopy. Journal of Microscopy 218, 52–61.
Gai, Y.H., Song, D.X., Sun, H.Y., Zhou, K.Y., 2006. Myriapod monophyly and relationships among myriapod classes based on nearly complete 28s and 18s rDNA sequences. Zoological Science 23, 1101–1108.
Glückstad, J., Palima, D., 2009. Generalized Phase Contrast. Number 1 in Springer Series in Optical Sciences, 146.
Goodman, J.W., 1988. Introduction to Fourier optics. Number 1 in Electrical engineering series.
Howells, M.R., Hitchcock, A.P., Jacobsen, C.J., 2009. Introduction: special issue on radiation damage. Journal of Electron Spectroscopy and Related Phenomena 170, 1.
Jefimovs, K., Vila-Comamala, J., Stampanoni, M., Kaulich, B., David, C., 2008. Beam-shaping condenser lenses for full-field transmission X-ray microscopy. Journal Synchrotron Radiation 15, 106.
Koditschek, D.E., Full, R.J., Buehler, M., 2004. Mechanical aspects of legged locomotion control. Arthropod Structure and Development 33, 251–272.
Marone, F., Hintermuller, C., Geus, R., Stampanoni, M., 2008. Towards real-time tomography: fast reconstruction algorithms and gpu implementation, pp. 555–561.
Mokso, R., Cloetens, P., Maire, E., Ludwig, W., Buffiere, J.Y., 2007. Nanoscale zoom tomography with hard X-rays using kirkpatrick-baez optics. Applied Physics Letters 90, 144104.
Neuhausler, U., Schneider, G., Ludwig, W., Meyer, M.A., Zschech, E., et al., 2003. X-ray microscopy in zernike phase contras mode at 4 kev photon energy with 60 nm resolution. Journal of Physics D: Applied Physics 36, 79–82.
Parkinson, D.Y., McDermott, G., Etkin, L.D., Le Gros, M.A., Larabell, C.A., 2008. Quantitative 3-D imaging of eukaryotic cells using soft X-ray tomography. Journal of Structural Biology 162, 380.
Regier, J.C., Schultz, J.W., Kambic, R.E., 2005. Pancrustacean phylogeny: hexapods are terrestrial crustaceans and maxillopods are not monophyletic. Proceedings Biological sciences 272, 395–4011.
Requena, G., Cloetens, P., Altendorfer, W., 2009. Submicrometer synchrotron tomography using kirkpatrick-baez optics. Scripta Materialia 61, 760–763.
Sakdinawat, A., Attwood, D., 2010. Nanoscale X-ray imaging. Nature Photonics 4, 840–848.
Schulz, H.N., 2006. The genus Thiomargarita, Number 6 in Prokaryotes. Springer-Verlag, Berlin.
Schulz, H.N., Brinkhoff, T., Ferdelman, T.G., Hernandez, M., Teske, A., et al., 1999. Dense population of a giant sulfur bacterium in namibian shelf sediments. Science 284, 493.
Schulz, H.N., Schulz, H.D., 2005. Large sulfur bacteria and the formation of phosphorites. Science 307, 416.
Stampanoni, M., Marone, F., Modregger, P., Pinzer, B., Thüring, T., et al. 2010. Tomographic Hard X-ray Phase Contrast Micro- and Nano-Imaging at TOMCAT. AIP Conference Proceedings 1266,13–17.
Stampanoni, M., Mokso, R., Marone, F., Vila-Comamala, J., Gorelick, S., et al., 2010. Phase-contrast tomography at the nanoscale using hard X-rays. Physical Review B 81, 140105.
Takeuchi, A., Suzuki, Y., Uesugi, K., 2011. Present status of the nanotomography system at BL47XU at SPring-8. AIP Conference Proceedings 1365, 301–304.
Teschke, M., Sinzinger, S., 2009. Phase contrast imaging: a generalized perspective. JOSA A 24, 1015–1021.
Tiegs, O.W., 1947. The development and affinities of the pauropoda, based on a study of pauropus silvaticus. Quarterly Journal of Microscopical Science 88, 275–336.
von Reumont, B.M., Meusemann, K., Szucsich, N.U., Dell'Ampio, E., Gowri-Shankar, V., et al., 2009. Can comprehensive background knowledge be incorporated into substitution models to improve phylogenetic analyses? A case study on major arthropod relationships. BMC Evolutionary Biology 9.
Zernike, F., 1934. Inflection theory of the cutting method and its improved form, the phase contrast method. Physica 1, 689.